UDC 551.558.1:551.576.11:551.509.313(213)

# NUMERICAL MODELS OF A TROPICAL CUMULUS CLOUD WITH BILATERAL AND AXIAL SYMMETRY [1]

F. W. MURRAY

The Rand Corporation, Santa Monica, Calif.

## ABSTRACT

Two versions of a numerical model for cumulus convection are compared. One is symmetrical about a vertical plane, the other about a vertical axis. It is found that the axisymmetric model grows more vigorously than the other and more realistically represents the relations between updraft and downdraft, the shape, and other characteristics. The previous findings of Ogura are generally confirmed and extended.

## 1. INTRODUCTION

Since the initial numerical experiments in atmospheric thermal convection by Malkus and Witt (1959) and Ogura (1962, 1963), a number of other models of the same general type have been proposed, each emphasizing one or another aspect of the problem. Among these are the models of Ogura and Charney (1962), Lilly (1962), Chou (1962), Chou et al. (1965), Li et al. (1964), Asai (1964*a*, 1964*b*), Murray and Anderson (1965), Nickerson (1965), Takeda (1965), Orville (1965, 1968), Amirov (1966*a*, 1966*b*), Inman (1966), Lebedev (1966), and Árnason et al. (1968). These models differ in many details, but nearly all of them have in common the property of two-dimensionality, the full extension to three dimensions being beyond the capacity of computers available during this period.

There have been two principal ways in which the third dimension was eliminated. In some cases Cartesian coordinates were used with the assumption that no property varies in the $y$-direction, whereas in others cylindrical coordinates were used with the assumption that no property varies in the azimuthal direction. Certain problems (for example, the squall line) are more properly formulated in Cartesian coordinates, but for modeling individual clouds the cylindrical formulation is more appropriate. However, the additional complexity of the cylindrical formulation has led some investigators to use the other, even when it is apparently less suited to the problem at hand. So far as has been ascertained, only Ogura (1963) has studied the same problem with both geometries, and it is on the basis of rather limited comparative data published by him that it has been assumed that the two schemes yield essentially similar results. It is the purpose of the present study to test this assumption further, and to do so it is desirable to make a more detailed comparison of axial and rectilinear symmetry in numerical cloud modeling.

Most of the models mentioned above are based on the Boussinesq approximation or the slightly more general anelastic equations, either of which permits the definition of a stream function and the derivation of a vorticity equation. A number of finite-difference schemes have been devised to solve this type of equation. The properties of these schemes have been extensively discussed in the literature (see, for example, Molenkamp 1968) and will not be further discussed here. Almost all of the practical schemes, however, solve the vorticity equation locally in the Eulerian sense, following which the stream function is found by inversion of an elliptic operator, usually by an iterative technique.

Several of the convection models treat a dry atmosphere. This approach can yield some interesting results, but it is much more useful to consider a moist atmosphere in which water can exist in at least the liquid and vapor phases. Murray and Hollinden (1966) have proposed a model that treats water in all three phases. It has been found that in atmospheric thermal convection, release of latent heat has more effect on buoyancy than any other single process. Some models assume pseudoadiabatic processes; that is, all condensed water is immediately dropped out. Hence a cloud parcel ascends moist adiabatically, but descends dry adiabatically without evaporation. Other models, including the one to be described herein, assume reversible processes; that is, all condensed water is carried with the air and is available later for evaporation. Still better is the assumption that only part of the condensate falls out as rain, but determination of what part this is to be is still a vexing problem. Precise treatment of rain would necessitate detailed modeling of microphysical processes, but to date no program has been developed that can handle both this and cloud-scale dynamics simultaneously; in all probability this must await the next generation of large parallel-processing computers. Several existing models, however, have parameterized precipitation mechanisms. The most successful parameterization of this type so far is the one developed by Kessler (1967); with some modification it is used by several cloud modelers. The model described herein, however, is based on reversible processes without fallout of rain.

The method developed by Ogura (1963) to handle moist air (and later adopted by several other investigators) is as follows: From the basic equations of hydrodynamics and thermodynamics, one derives a prediction equation for the component of vorticity perpendicular to the vertical

[1] Research supported under Contract E-37-67(N) with the Environmental Science Services Administration and under Project RAND of the U.S. Air Force

plane in which motion occurs and conservation equations for total water substance and specific entropy of moist air. The finite-difference analogs of these equations are solved at each grid point, and the temperature is then determined from the specific entropy by one of two methods, depending on whether or not the air is saturated. Total water substance is then partitioned between liquid and vapor on the assumption that any excess of mixing ratio over the saturation value represents liquid water.

In the present investigation a somewhat different method was employed. The vorticity equation and its solution are essentially the same as in Ogura's model, but the thermodynamic equations are solved in a Lagrangian manner. The rationale for this is that the physical processes relating to condensation and evaporation are usually described in terms of changes occurring in individual parcels. The various processes are interrelated in a highly implicit way, but if attention is confined to an individual parcel, they can be treated serially while maintaining the error within acceptable bounds. The Lagrangian approach is conceptually more straightforward than the Eulerian in this case, and in practice it has been found to be more stable computationally. One drawback is that the smoothing resulting from the necessary interpolation acts like an implicit eddy diffusion. This effect, however, appears to be small enough not to be troublesome. Quantities such as total water substance are not exactly conserved, but the loss is quite small.

## 2. THE MODEL

The Boussinesq equation of motion for moist air (valid if convection is confined to a layer a few kilometers in depth) is

$$\frac{\partial \mathbf{v}}{\partial t}=-\mathbf{v}\cdot\nabla\mathbf{v}-\bar{\alpha}\nabla p'+g\left(\frac{T^{*\prime}}{\bar{T}^{*}}-r_l\right)\mathbf{k}+\nu_M\nabla^2\mathbf{v}. \tag{1}$$

The symbols are defined in the appendix. The virtual temperature is defined by

$$T^*=\frac{1+r_v/\epsilon}{1+r_v}\,T. \tag{2}$$

The Boussinesq equation of continuity is

$$\nabla\cdot\mathbf{v}=0. \tag{3}$$

If one takes the curl of equation (1) and uses (3), there results

$$\frac{\partial \boldsymbol{\omega}}{\partial t}=\nabla\times(\mathbf{v}\times\boldsymbol{\omega})+\nabla\times B\mathbf{k}-\nu_M\nabla\times(\nabla\times\boldsymbol{\omega}) \tag{4}$$

where

$$\boldsymbol{\omega}=\nabla\times\mathbf{v} \tag{5}$$

and

$$B=g\left(\frac{T^{*\prime}}{\bar{T}^{*}}-r_l\right). \tag{6}$$

Two different two-dimensional models derived from equation (4) will be discussed. The first uses a Cartesian coordinate system $(x,y,z)$ and proceeds on the assumption that the component of velocity and the variation of all properties in the $y$-direction are zero; this is the rectilinear model. The second uses a cylindrical coordinate system [2] $(x,\theta,z)$ and proceeds on the assumption that the tangential component of velocity is zero and all properties are independent of $\theta$; this is the axisymmetric model. Subscripts $R$ and $A$ will be used to denote variables pertaining to the rectilinear and axisymmetric models, respectively.

Because of the incompressibility implied by equation (3), it is possible to express the wind components in terms of a stream function, as follows:

$$\left.\begin{aligned} u&=-\frac{\partial\psi_R}{\partial z}=-\frac{1}{x}\frac{\partial\psi_A}{\partial z}\\ w&=\frac{\partial\psi_R}{\partial x}=\frac{1}{x}\frac{\partial\psi_A}{\partial x}\end{aligned}\right\}. \tag{7}$$

The horizontal component of vorticity is

$$\eta=-\left[\frac{\partial w}{\partial x}-\frac{\partial u}{\partial z}\right] \tag{8}$$

or

$$\left.\begin{aligned} \eta_R&=-\left[\frac{\partial^2\psi_R}{\partial x^2}+\frac{\partial^2\psi_R}{\partial z^2}\right]\\ \eta_A&=-\left[\frac{\partial}{\partial x}\left(\frac{1}{x}\frac{\partial\psi_A}{\partial x}\right)+\frac{1}{x}\frac{\partial^2\psi_A}{\partial z^2}\right]\end{aligned}\right\}. \tag{8a}$$

The transverse or tangential component of equation (4) is then

$$\left.\begin{aligned} \frac{\partial\eta_R}{\partial t}&=-\left[\frac{\partial}{\partial x}(u\eta_R)+\frac{\partial}{\partial z}(w\eta_R)\right]-\frac{\partial B}{\partial x}+\nu_M\left[\frac{\partial^2\eta_R}{\partial x^2}+\frac{\partial^2\eta_R}{\partial z^2}\right]\\ \frac{\partial\eta_A}{\partial t}&=-\left[\frac{\partial}{\partial x}(u\eta_A)+\frac{\partial}{\partial z}(w\eta_A)\right]-\frac{\partial B}{\partial x}\\ &\quad+\nu_M\left[\frac{\partial}{\partial x}\left\{\frac{1}{x}\frac{\partial}{\partial x}(x\eta_A)\right\}+\frac{\partial^2\eta_A}{\partial z^2}\right]\end{aligned}\right\}. \tag{9}$$

If at a given time $\psi$ (which determines $u$, $w$, and $\eta$) and $T$, $r_v$, and $r_l$ (which collectively determine $B$) are known at each grid point, (9) can be solved to determine $\eta$ at each grid point at a later time, following which (8a) can be solved for $\psi$ at the later time. The latter can be done as a Dirichlet problem with $\psi=0$ on all boundaries, a condition equivalent to the requirement that no air pass through any of the boundaries. (The boundaries are taken to be two horizontals, one representing the ground and one an undisturbed upper level, and two verticals, one representing an axis of symmetry and one a lateral wall enclosing the region of convective circulation.)

These computations are all accomplished with use of central differences in space and leapfrog central differences in time (forward differences for the first time step). This method, according to Molenkamp (1968), introduces less pseudo diffusion than the upstream method used by Ogura and by Orville.

[2] The notation $x$ is used here rather than the more conventional $r$ to facilitate comparison with the Cartesian system.

370-724 O—70——3

The Lagrangian part of the scheme encompasses the determination of $T$, $r_v$, and $r_l$ at each grid point at the later time. This is done in several steps, as follows:

1) Using the values of $u$ and $w$ at a grid point and its neighbors at the beginning and end of the time step, a single-time-step backward trajectory is computed to determine the point of origin of the air parcel that is found at the grid point at the end of the time step.

2) Values of temperature, humidity, etc. at the point of origin at the beginning of the time step are found by interpolation among the four surrounding grid points.

3) If the air parcel at the point of origin is undersaturated in the presence of liquid water or is supersaturated, an adjustment is made to $T$, $r_v$, and $r_l$ to rectify this condition. Since the adjustment is small, it is assumed to occur instantaneously at constant pressure. The saturation mixing ratio is given by

$$r_s=\frac{\epsilon e_s}{p-e_s} \tag{10}$$

and the saturation vapor pressure by Tetens' formula:

$$e_s=6.1078\ \exp\left[\frac{a(T-273.16)}{(T-b)}\right] \tag{11}$$

with $a=17.2693882$ and $b=35.86$. Differentiation and combination of equations (10) and (11) yield

$$dr_s=\frac{r_s(\epsilon+r_s)a(273.16-b)}{\epsilon(T-b)^2}\,dT; \tag{12}$$

but the change of temperature due to condensation or evaporation is

$$dT=\frac{L}{c_p+r_vc_{pv}+r_lc_w}\,dr_l=-\frac{L}{c_p+r_vc_{pv}+r_lc_w}\,dr_v. \tag{13}$$

The object of the adjustment is to make $r_s$ and $r_v$ equal; hence

$$r_s+dr_s=r_v+dr_v. \tag{14}$$

Combination of (12), (13), and (14) yields

$$dr_l=-dr_v=\frac{r_v-r_s}{1+\dfrac{r_s(\epsilon+r_s)a(273.16-b)L}{\epsilon(T-b)^2(c_p+r_vc_{pv}+r_lc_w)}}. \tag{15}$$

The static adjustment consists of applying (15) to $r_l$ and $r_v$ and equation (13) to $T$. If $r_v<r_s$, the adjustment can be no greater than $r_l$, (15) notwithstanding.

4) If the parcel is now exactly saturated, a dynamic adjustment is made to $T$, $r_v$, and $r_l$. Under the assumption of conservation of equivalent potential temperature, it can be shown (see Berkovsky 1960) that the rate of change of saturation mixing ratio is

$$\frac{dr_s}{dt}=\frac{1-\dfrac{c_pT-Lr_s}{\epsilon L}}{L+\dfrac{c_pRT^2}{Lr_s(\epsilon+r_s)}}\,gw. \tag{16}$$

If $r_v=r_s$, then $dr_s/dt=-dr_v/dt=dr_l/dt$, and so equation (16) gives the rate of condensation, and (13) gives the rate of change of temperature due to conversion of latent heat. Thus, one can determine the change of $T$, $r_v$, and $r_l$ due to condensation or evaporation as the parcel moves from its point of origin to the grid point.

5) The temperature of the parcel also changes adiabatically at the rate $-gw/c_p$; this must be taken into account whether or not step 4 was applicable. At this stage the modified values of $T$, $r_v$, and $r_l$, which result from the application of the various adjustments to the values determined for the point of origin at the beginning of the time step, are preliminary values for the grid point at the end of the time step.

6) Fickian eddy diffusion is assumed, so terms of the form $\nu_T\nabla^2T'$, $\nu_r\nabla^2r_v$, and $\nu_r\nabla^2r_l$ must be included in the rates of change of temperature, mixing ratio of vapor, and mixing ratio of liquid. These terms are evaluated in the Eulerian manner at each grid point at the beginning of the time step and are now used to adjust the grid-point values of $T'$, $r_v$, and $r_l$ at the end of the time step.

7) Because of nonlinearities in most of the processes, there may at this stage be points at which the air is undersaturated in the presence of liquid water or is supersaturated. If so, the adjustment of step 3 is again applied, this time at the grid point.

## 3. INITIAL CONDITIONS

It is assumed that initially the atmosphere is at rest and horizontally homogeneous. Ordinarily the variation of $T$ and $r_v$ in the vertical is in accordance with some actual atmospheric sounding, and $r_l$ is taken to be zero everywhere. Unless some impulse is applied, the right-hand side of (9) is identically zero, and nothing can happen. The customary impulse used for this type of model is a bubble of increased temperature. This makes $B$ no longer independent of $x$, so $\eta$ can grow. The rising motion so induced in the center of the bubble can lead to condensation and conversion of latent heat to sensible heat, making the process self-sustaining. Something like this process is thought to occur in nature when a cumulus cloud is generated, but in one respect this process is unrealistic. The arbitrary initial increase in temperature within the bubble is accompanied by a decrease in relative humidity, delaying the onset of condensation and ensuring that the cloud develops in the driest part of the region.

It is perhaps more realistic to introduce a humidity impulse rather than a temperature impulse. There is then a horizontal gradient of virtual temperature (though not of temperature) to make the right-hand side of (9) nonzero. If the impulse is such as to produce saturation within the bubble, condensation can start immediately. Humidity impulses have been studied both theoretically and observationally by Vul'fson (1964), who found them to be of great importance, especially in convection over a water surface. This is the type of impulse used in the present study.

## 4. DISCUSSION

Ogura (1963) presented results of several runs with a model having axial symmetry. He used a 30-by-30 grid, and for lateral boundary conditions he required that both $u=0$ and $\partial w/\partial x=0$ at the central axis and at the outer wall. One run having a basic atmosphere with a conditionally unstable lapse rate and saturation throughout was repeated with rectilinear geometry, but with a 20-by-20 grid and cyclic lateral boundary conditions.

The main points noted by Ogura in comparing the two runs were:

a) The strength of the downdraft outside the cloud is stronger in the rectilinear model than in the axisymmetric. At 8 min the ratios of maximum downdraft to maximum updraft were .25 and .06, respectively.

b) The heating of the subsiding air produced a temperature gradient such that a cell with reversed circulation appeared below the cloud in the rectilinear model, but not in the axisymmetric.

c) The greater excess temperature produced in the downdraft of the rectilinear model resulted in appearance of a region of positive vorticity. This did not occur with the axisymmetric model.

It is possible that Ogura's use of different boundary conditions and grid dimensions contributed to the different results noted in the models with the two geometries. In order to avoid this possibility in the present investigation, runs were made with the two geometries using identical initial data, impulses, boundary conditions, and grid dimensions. The initial sounding used was one from San Juan, Puerto Rico, for a day on which well-developed cumuli were observed in the region. Its plot on a skew-T, log $p$ form is shown in figure 1. A humidity impulse was chosen so that initially there was slight supersaturation near the central axis and the convective condensation level; hence condensation commenced immediately, and the model cloud grew vigorously. The initial impulse is illustrated in figure 2.

The most obvious difference in the response of the axisymmetric and rectilinear models is that the former developed much faster and more strongly. This is apparent from figure 3, which shows the magnitude of the maximum updraft as a function of time. By 8 min the axisymmetric updraft was twice as strong as the rectilinear, and it continued to increase rapidly, reaching a maximum of 17 m sec$^{-1}$ by about 31 min. By contrast, the updraft of the rectilinear model did not quite reach 2 m sec$^{-1}$ by 30 min, at which time it showed signs of leveling off. Computation of the rectilinear model was not carried into the decaying stage, but the axisymmetric model was run out beyond 40 min. After 32 min the main updraft diminished as precipitously as it had increased, vanishing after 38 min. By then, however, a secondary updraft of 5–7 m sec$^{-1}$ had developed in the lower part of the cloud, suggesting a pulsation in cloud growth.

The relatively stronger development of the axisymmetric updraft is also reflected in the height at which the

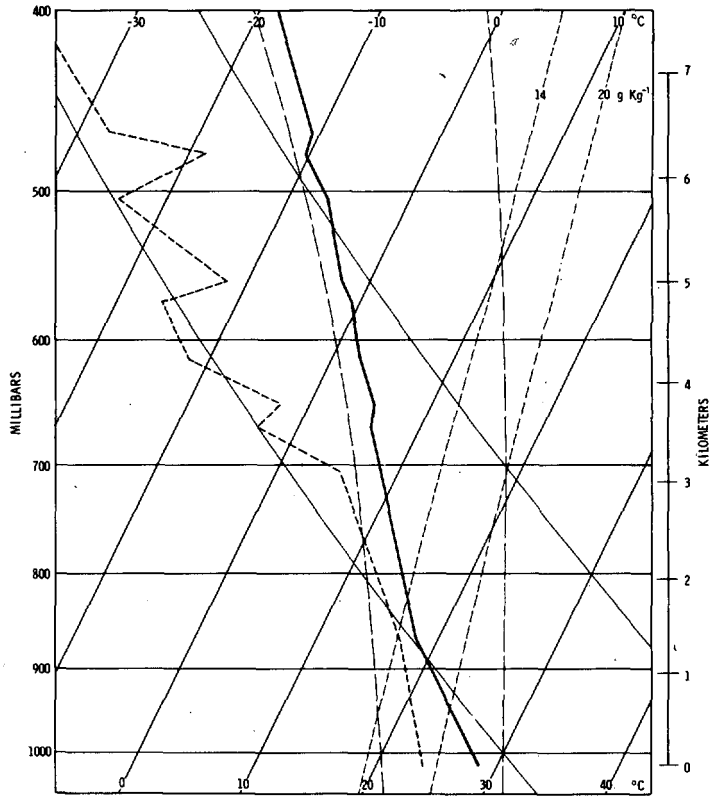


FIGURE 1.—Sounding for San Juan, Puerto Rico, at 2300 GMT on Aug. 20, 1963.

maximum occurred, shown in figure 4. Both maxima started at 1200 m, but by 28 min the rectilinear maximum had risen only to 1700 m, while the axisymmetric maximum had reached 3500 m. The latter center continued to rise even after its strength diminished, and just before it vanished at 40 min it was at 4400 m. The altitude of the maximum updraft agrees well with that of the maximum of liquid water content, as can be seen from comparison of figures 4 and 5.

The relative growth rates of the two models could be predicted qualitatively from the nature of the two geometries. Under the assumption that the horizontal area within radial distance $X$ is $\pi X^2$ for the axisymmetric model and $2XY$ for the rectilinear model, where $Y$ is some distance along the $y$-axis, one can determine that if there is updraft from the axis out to $X_1$ and thereafter downdraft out to $X_2$, the proportion of the total horizontal area occupied by updraft is $X_1^2/X_2^2$ for the axisymmetric model and $X_1/X_2$ for the rectilinear. In the present experiment, $X_2=5800$ m for both cases, whereas $X_1$ is typically 800 m for the axisymmetric case and 600 m for the rectilinear. Thus the updraft covers 2 percent of the total area in the axisymmetric case and 10 percent in the rectilinear. Obviously, if the two updrafts are to transport similar amounts of air through a given level, that of the axisymmetric model must be considerably stronger than the other. It should be remarked, however, that in both models most of the downdraft is concentrated near the evaporat-

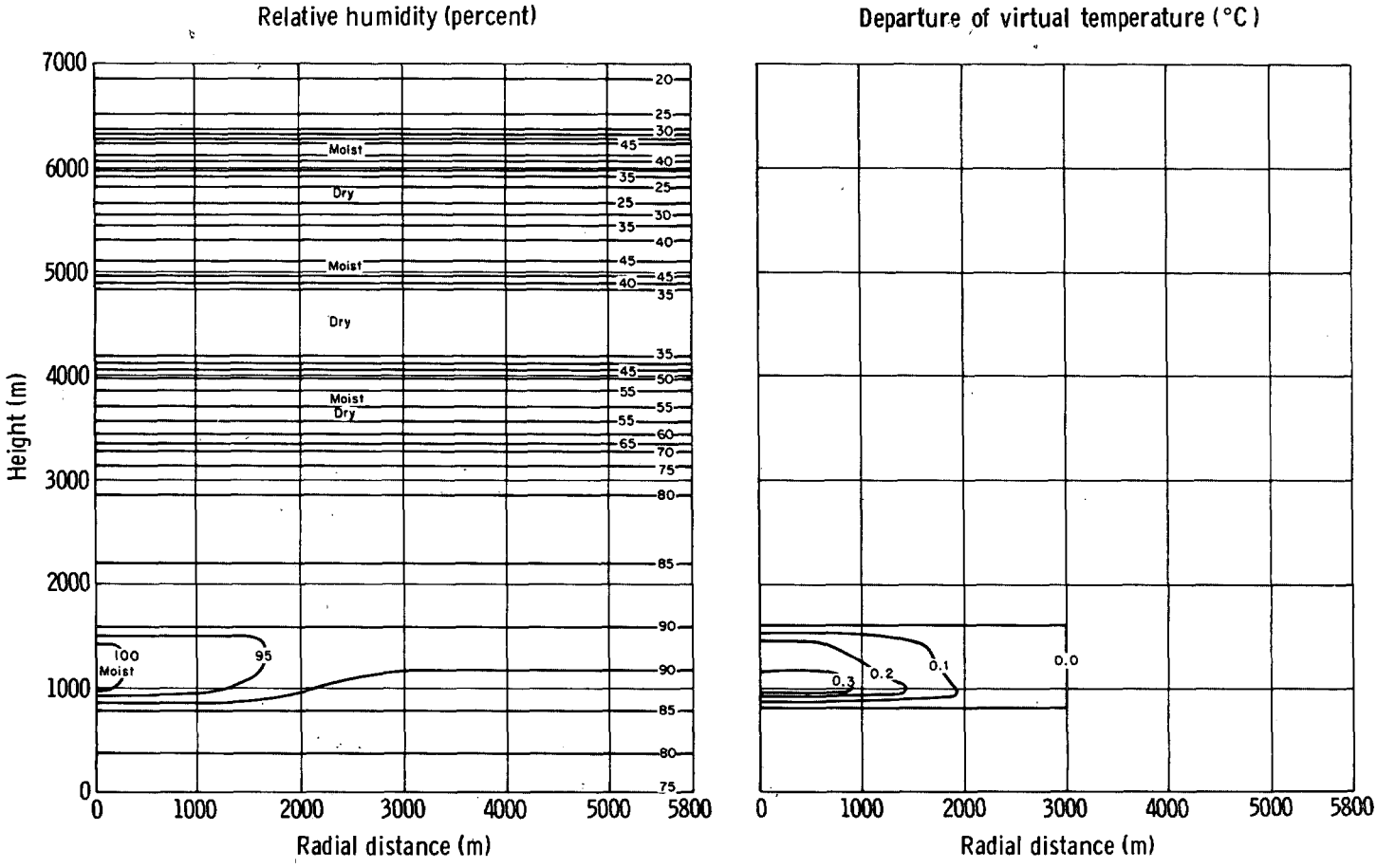


FIGURE 2.—Distribution of relative humidity and departure of virtual temperature from the basic state at initial time, including the impulse.

ing edge of the cloud, and the remainder of the downdraft area has a very slight vertical motion, and even some pockets of weak updraft.

In his initial exposition of the slice method, Bjerknes (1938) showed that the ratio of updraft to downdraft area must be small, and in an elaboration of that work, Petterssen (1939) suggested that 10 percent might be a reasonable figure, although he did not express high confidence in that estimate. However, it agrees with the present results for the rectilinear model. Recently, Krishnamurti (1968) determined by a study of total moisture convergence over an area of synoptic scale in the Caribbean and by airborne radar observations that 1 percent of the total area was covered by active convective cloud elements. This agrees with results of the axisymmetric model in the present experiment and offers a degree of confirmation of the superiority of that model in this respect.

One difficulty that occurs throughout this problem is the mathematical singularity on the central axis in the axisymmetric model. This has caused the greatest trouble in the evaluation of $w$ from (7) where $x=0$. The best method that has been found is to assume, with Ogura, that $\partial w/\partial x=0$ at $x=0$ (a reasonable assumption for axial symmetry) whereby it is easily shown that $w=\partial^2\psi_A/\partial x^2$ at $x=0$. With this formulation, the magnitude of $w$ seems to increase sharply, by comparison with the rectilinear model, over the last grid interval as the axis is approached, but not so sharply as with other axisymmetric formulations. The maximum updrafts shown in figure 3 are all on the central axis, but the general nature of figure 3 would not be changed if the magnitude of the maximum updraft for all grid points other than those on the central axis had been plotted instead. The effect at 29 min would be to reduce the value from 16.9 m $sec^{-1}$ to 6.9 m $sec^{-1}$ in the axisymmetric model and from 2.1 m $sec^{-1}$ to 0.8 m $sec^{-1}$ in the rectilinear model. These points are indicated on the figure by the symbol x.

Presumably Ogura used the same formulation for $w$ on the central axis. His figure 3 (at 14 min) shows the updraft decreasing from over 12 m $sec^{-1}$ on the central axis to zero near 600 m. The present model shows almost the same gradient at 26 min, but with some indication that the gradient over the first grid interval is somewhat larger than Ogura's. The difference may be due to the fact that in the solution of the vorticity gradient Ogura's model had more implicit eddy diffusion than the present

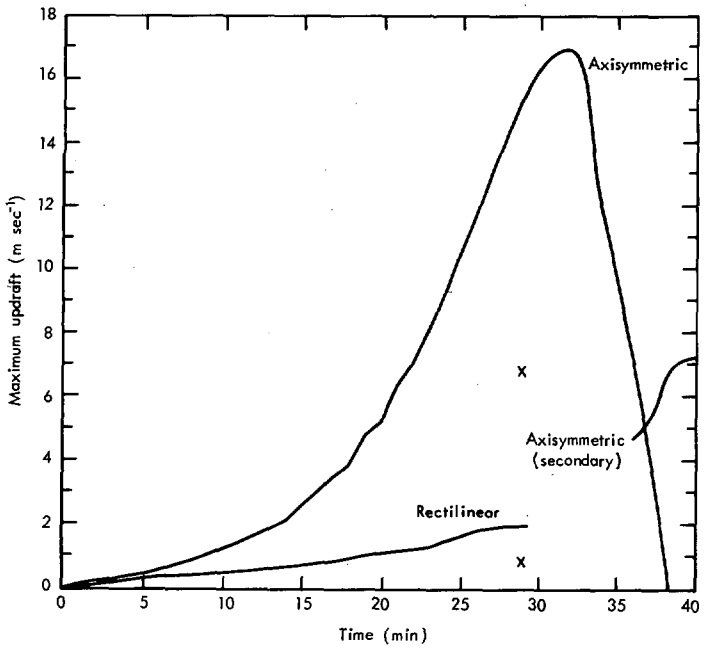


FIGURE 3.—Magnitude of maximum updraft.

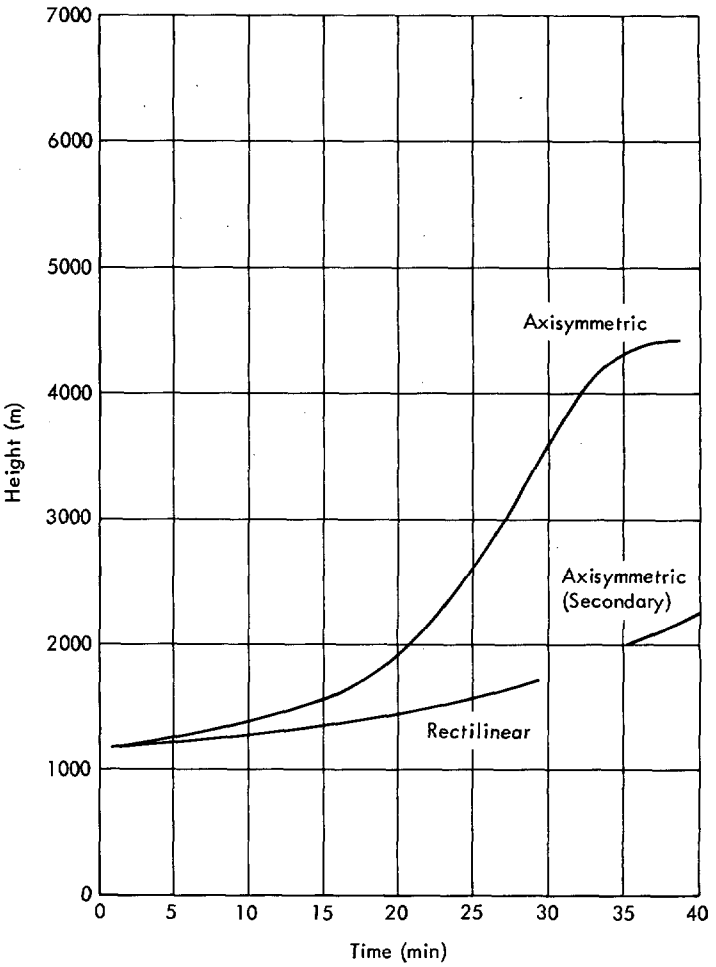


FIGURE 4.—Height of maximum updraft.

model, but equal explicit eddy diffusion. This is considered further in the discussion of entrainment later in this paper.

A simplified and qualitative study of the equations also will show that there is a sort of feedback mechanism that seems to ensure that the updraft of the axisymmetric model will grow faster than that of the rectilinear. (This mechanism probably has its counterpart in real clouds.) The built-in convergence of the cylindrical coordinate system acts to produce an updraft that is initially stronger than the downdraft. When condensation occurs, there is a considerable increase of temperature, and the contribution to (9) of the buoyancy term becomes large in the limited region of the cloud. This leads to a stronger updraft, more condensation, and so on. Thus the difference due merely to geometry is magnified. Between the cloud edge and the subsidence temperature maximum, however, the effect of the buoyancy term is negative, but it is not enhanced by condensation or evaporation. Moreover, the convergence of the coordinate systems is less, and the two models are more nearly alike.

The question arises as to whether the strong updraft of the axisymmetric model or the weak updraft of the rectilinear model is the more realistic. A rule of thumb, based on observations of real clouds, is that the cloud top rises at half the speed of the updraft. The rate of rise of the model cloud top can be determined from the slope of the upper part of the curves of figure 5, which is a time section of mixing ratio of liquid on the central axis. The results of this calculation, together with several other properties of the two simulated clouds after 25 min of growth (at which time the axisymmetric cloud top began to rise at its maximum rate), are listed in table 1.

From table 1 the ratio of updraft to rate of rise of cloud top is 3.7:1 for the rectilinear model and 3:1 for the axisymmetric. Both ratios are a little larger than would be expected from the rule of thumb, but if the updrafts were horizontally averaged across the simulated clouds rather than taken on the axis, the ratios would be near 2:1. This suggests that the updraft of each model is appropriate to its rate of growth. The axisymmetric model, despite a substantially stronger updraft, has a slightly smaller ratio of updraft to rate of rise.

Ogura did not discuss the actual magnitude of the vertical currents but only the ratio of maximum downdraft to maximum updraft. These ratios for the growth stage of the cloud in the present experiment are shown in figure 6. As Ogura reported, the ratio for the rectilinear model is substantially larger than that for the axisymmetric model, but figure 6 shows that the ratios are not at all constant. Both show a marked decrease for the first 7 or 8 min, followed by a marked increase. If isotachs of the vertical component of velocity or streamlines are plotted for each time step, it is found that the center in which the maximum downdraft is located during

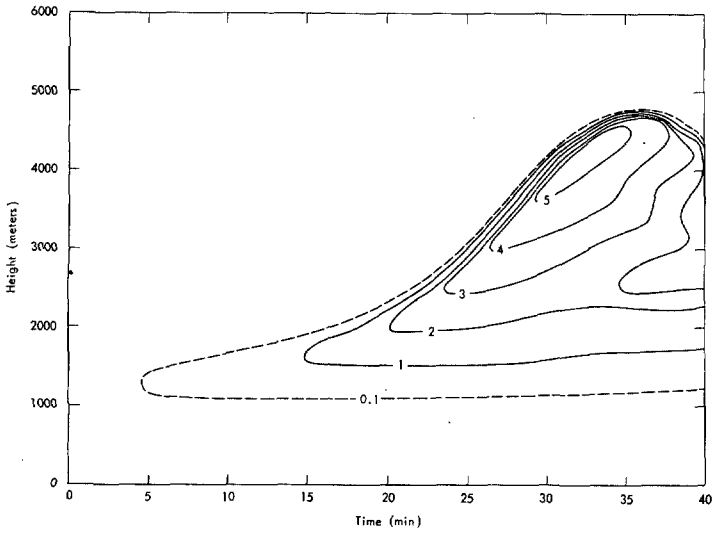


FIGURE 5.—Time section of the mixing ratio of liquid on the central axis, axisymmetric model.

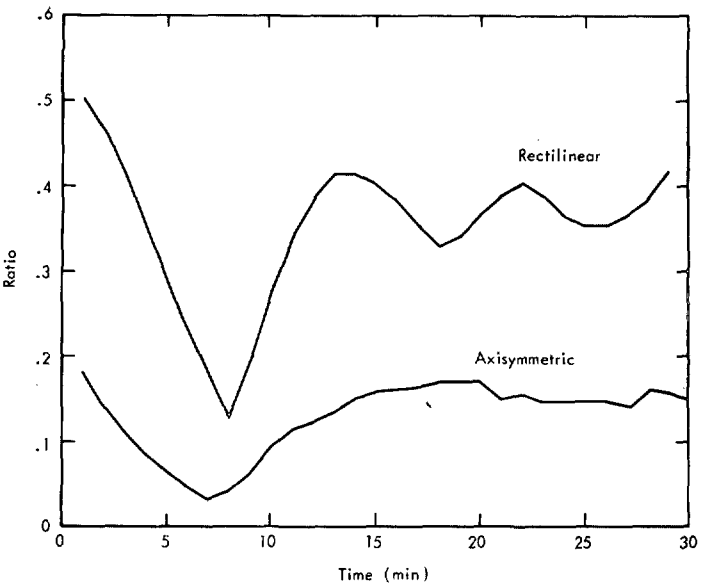


FIGURE 6.—Ratio of the magnitude of maximum downdraft to the magnitude of maximum updraft.

TABLE 1.—*Some properties of the simulated cloud at 25 min*

| | Rectilinear | Axisymmetric |
|---|---|---|
| Cloud top (km) | 2.0 | 3.2 |
| Rate of rise of cloud top (m sec $^{-1}$) | 0.46 | 3.56 |
| Updraft (m sec$^{-1}$) | 1.7 | 10.6 |
| Mixing ratio of liquid (gm kg$^{-1}$) | 0.9 | 3.6 |
| Temperature excess (°C) | 0.5 | 1.8 |

the first 7 or 8 min is not the same as that for later times. Initially, there is a single-cell circulation pattern centered near $x=1600$ m, with updraft closer to the axis and downdraft further from it. As the simulated cloud develops, this cell strengthens and its center moves inward and upward, but a weak secondary center develops and moves outward. At first the maximum downdraft is outside the secondary center, but gradually the downdraft between the centers increases, and after about 8 min it becomes the dominant downdraft. Thereafter the maximum updraft and maximum downdraft are closely related to each other and to the area of condensation, although secondary maxima and minima occur at various spots throughout the computational region. Hence after about 10 min, comparisons should be significant.

The ratios shown in figure 6 are roughly comparable to the ratios of .25 and .06 reported by Ogura at 8 min, but they tend to be somewhat higher. The ratio of the ratios in Ogura's experiment was 4:1, whereas in the present experiment it is in the range 3:1 to 2:1. These differences, which do not appear to be significant, can be ascribed to differences in the models, or more particularly to differences in initial data. What is important is that the ratio of maximum downdraft to maximum updraft is larger in the rectilinear model than it is thought to be for actual clouds, whereas it has a more realistic value in the axisymmetric model.

Study of the streamlines and isotachs has disclosed no apparent reason for the regular oscillation of the upper curve of figure 6 after 8 min, other than that it is connected in some way with the gravity waves of period near 10 min that are typical of this convective model. The waves are probably the consequence of the assumption of a rigid upper boundary. It is not known why the lower curve of figure 6 fails to show the same oscillation.

Plots of temperature departure as a function of position at various times (for example, fig.7[3]) show a strong maximum in the region of condensation surmounted by a cap of temperature deficit resulting from forced lifting of yet-unsaturated air above the active cell. This cap tends to extend downward in a narrow band along the edge of the cloud, where evaporation is taking place. Farther out there is another maximum, strong in the rectilinear model and weak in the axisymmetric, related to subsidence of relatively dry air. It is this temperature excess together with the temperature deficit associated with dry-adiabatic ascent below the cloud that causes the development of the reverse-circulation cell mentioned by Ogura. In the present experiment this cell appeared both with the axisymmetric and the rectilinear models, but it is very weak in both (fig. 8). If anything, it is a little stronger in the axisymmetric model, but so are all other circulations. A strong reverse cell has appeared in previous runs of the rectilinear model, however, when the initial impulse was a temperature excess as in Ogura's experiment. It is believed that

[3] Figures 7 through 13 are taken from computer-constructed charts. On them small squares indicate grid points of maximum value relative to adjacent surrounding grid points, and small circles represent relative minima in the same sense. The ordinate is height and the abscissa is radial distance, both in meters. The edge of each square block is five mesh lengths.

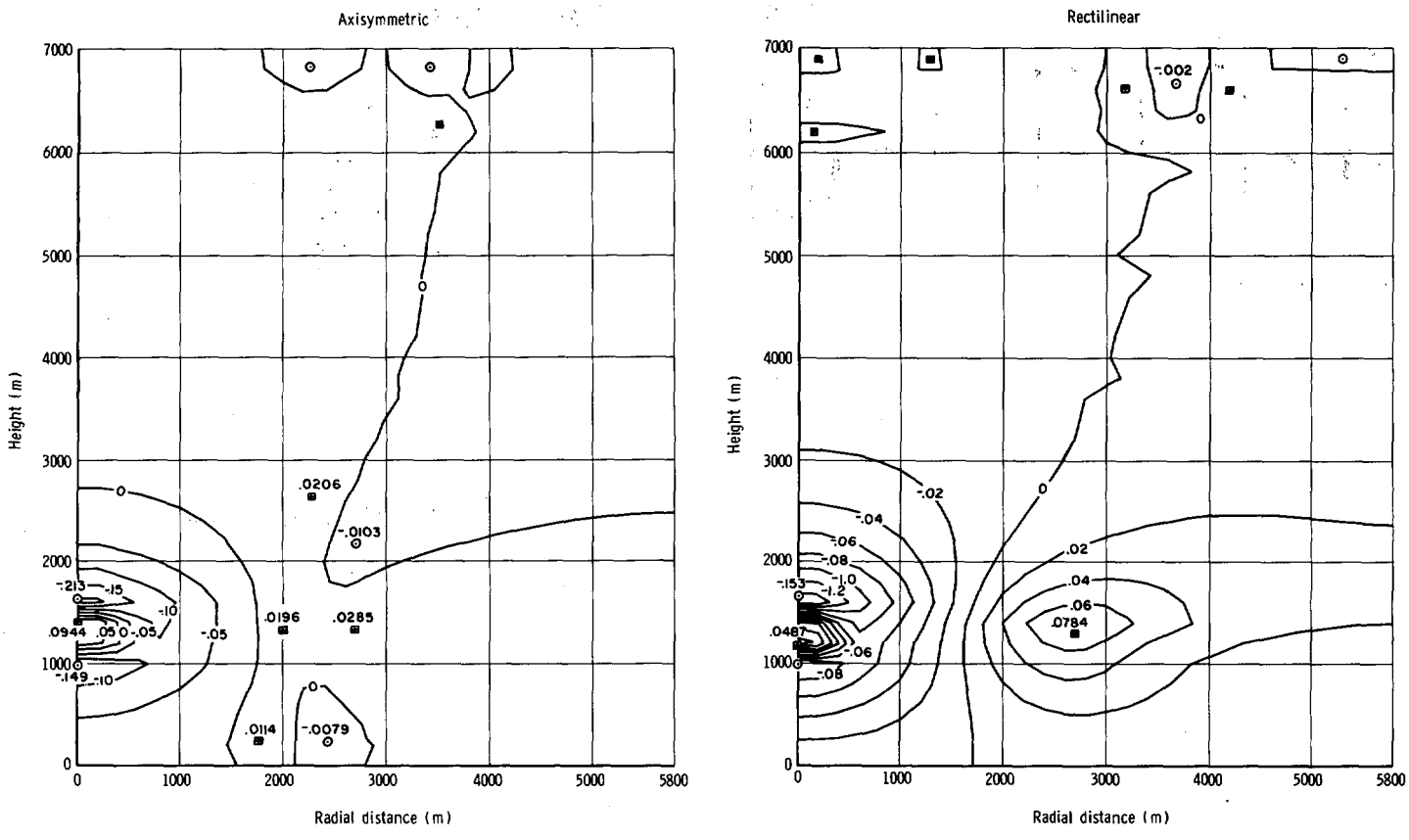


FIGURE 7.—Temperature departure at 5 min, case of weak development.

its failure to appear strongly here is related to the type of impulse.

The center of excess temperature in the subsiding air has another effect that has been evident in most models of this type. As the model cloud develops, its active vortex moves upward, leaving a relatively passive mass of cloud at lower levels. The inflow associated with the vortex brings in warm dry air, causing that portion of the cloud to evaporate. There frequently results a rather globular cloud in the region of the active vortex, with a narrow stem extending down along the central axis. Because the rectilinear model has a stronger subsidence temperature excess, this effect is particularly noticeable in models with such a geometry; see Ogura's figure 20. The same action occurs in the axisymmetric model, but it is less intense. The effect is illustrated in figure 9, which is taken from a case with a more extensive initial impulse than that of the other illustrations in this report, and consequently with more vigorous development. In many instances the stem of the cloud in the rectilinear model is only a single mesh unit wide.

The continued maintenance of a narrow stem below the active part of the cloud brings one to a consideration of entrainment. In other types of cloud models an explicit entrainment term is included, which generally has the effect of mixing some of the air from a uniform environment with uniform cloud air, resulting in a cloud with new uniform properties. In the type of model considered here, the cloud is not an entity, but only a collection of grid points having in common the single property $r_l>0$. Hence, the ordinary type of entrainment term is not pertinent.

There are, however, two types of entrainment in this model. Dynamic entrainment refers to the process whereby a particle trajectory leads from a point outside the cloud to a point within it. This occurs when a parcel without liquid water reaches, through some process, a state of saturation, and condensation commences. Such a parcel has then been entrained. Turbulent entrainment is more comparable to the normal notion of entrainment—a form of mixing. In this model it can occur explicitly through the Fickian eddy diffusion terms or implicitly through the finite-differencing and through the interpolation required by the Lagrangian part of the computation. The distinction between the two types of entrainment is really one of scale. Dynamic entrainment is of cloud scale; turbulent entrainment is of subgrid scale.

Since $u=0$ at $x=0$, dynamic entrainment cannot occur along the central axis (except trivially at the bottom and top of the cloud). It can, however, occur at all other points about the cloud, and it creates the mushroom effect noted above by causing evaporation at points away from the axis. Turbulent mixing, on the other hand, can

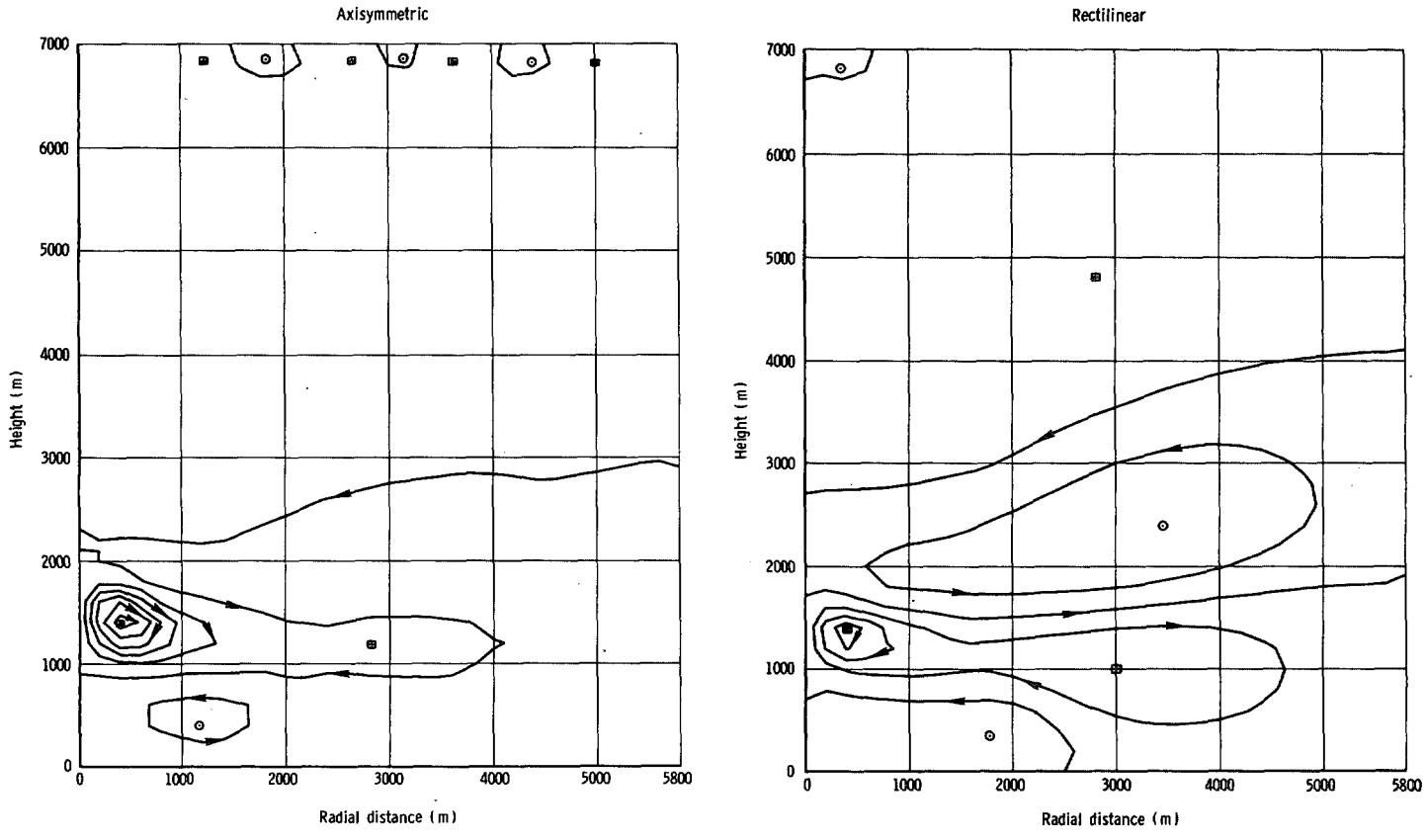


FIGURE 8.—Streamlines at 12 min, case of weak development.

occur at any point of the cloud, including the central axis, and it may be the key to control of unrestrained growth both in the model and in nature. The basic sounding used in the present experiment, the lower part of which is shown in figure 1, is only slightly less stable and more humid than the mean August Caribbean sounding. A few cumulonimbus clouds were observed over the ocean at the time of this sounding, but most of the clouds grew only to moderate heights (Simpson et al. 1965). Yet the parcel method, which does not allow for entrainment, would predict that any disturbance would grow to the tropopause. It appears that nature uses entrainment to check runaway convection.

Since in the present experiment the axisymmetric cloud topped out at 4.8 km (as can be seen from fig. 5), and the rectilinear cloud was much smaller, whereas the sounding indicates that without entrainment the cloud should extend to the tropopause, it is desirable to investigate the ways in which entrainment can affect the model cloud growth. It has been noted that dynamic entrainment cannot occur on the central axis, where the greatest cloud height was reached. It can occur at off-axis points, and the resulting evaporation will tend to reduce the cloud diameter. The evaporative cooling will then produce a horizontal gradient of virtual temperature, thereby enhancing the buoyancy, which is opposite to the effect generally attributed to entrainment. This should be minor, however.

On the other hand, turbulent entrainment tends to reduce the gradients of the various properties, thereby diminishing buoyancy. In the present model there are explicit terms for eddy diffusion of water substance, temperature excess, and vorticity. Moreover, there is implicit diffusion introduced by the finite-difference scheme. Molenkamp (1968) showed that Ogura's upstream-differencing scheme introduced implicit eddy diffusion equivalent to that caused by an explicit coefficient of 40 $m^2$ $sec^{-1}$. Coincidentally, that is the same value of the coefficient that Ogura had found to be the smallest that gave discernible difference on the computations—perhaps because of the masking by the implicit effect. It is also the value used in the present experiment. The central-difference scheme has less implicit eddy diffusion than the upstream scheme, so with regard to the velocity field Ogura's model was more strongly damped than this one. On the other hand, the Lagrangian computation for temperature and water substance used here probably has at least as much implicit eddy diffusion as Ogura's method.

It is conceivable that the damping due both to turbulent entrainment and to the retention of all condensed water is a bit too great. Dr. Joanne Simpson (1968) has suggested

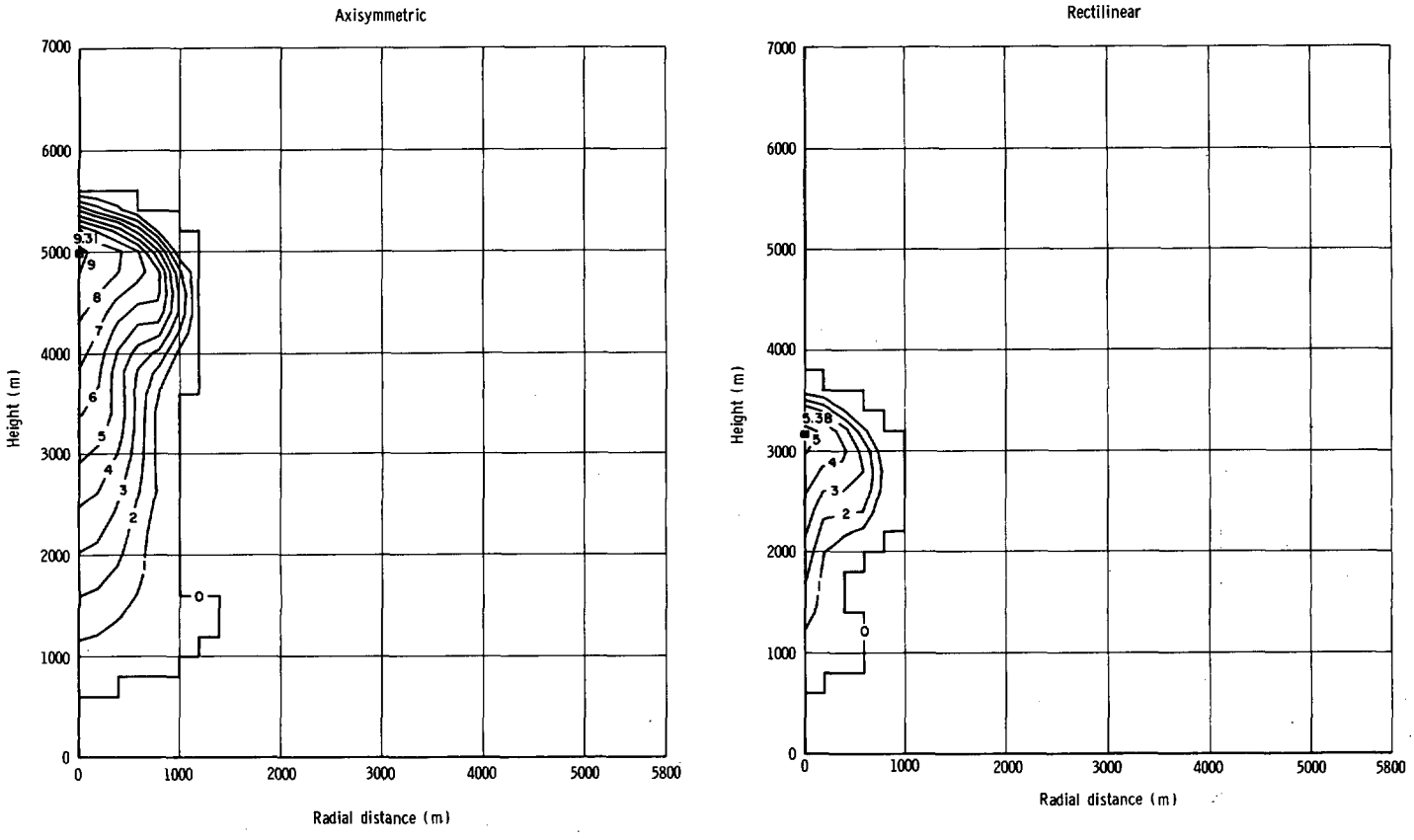


FIGURE 9.—Mixing ratio of liquid at 16 min, case of strong development.

that with this sounding the cloud should top out between 7 and 8 km. Because of limitations of core storage of the hitherto-available computer (IBM 7044) the computation region could not be extended above 7 km in order to make a run with less damping unless the mesh length was increased. Since the mesh length is already rather large (200 m), this was not considered desirable. Incidentally, Ogura's computation region was only 3 km deep, and the simulated cloud soon impinged on the ceiling, making further computation of limited usefulness.

Some types of models, such as that of Simpson et al. (1965), require specification of cloud diameter, which controls the rate of entrainment, and consequently determines the height to which the cloud will rise. In the present model, by contrast, cloud diameter is one of the results that come out of the computation. It might be related to the diameter of the initial impulse, but in the many runs that have been made it has invariably been less than that diameter. It is interesting to note that with identical initial impulses the diameter of the axisymmetric cloud turns out to be a little greater than that of the rectilinear cloud. The formulation of this model, however, differs from those having an entrainment law and does not ensure that there will be lesser entrainment for a greater diameter, except in that the wider simulated cloud has many more interior grid points, but only a few more boundary grid points, so that the ratio of mass entrained to total mass is less than for the narrower cloud. This, however, is not a quantity that is considered by the model.

Ogura's observation of the development of a center of positive vorticity in connection with the temperature maximum associated with subsidence seems not to be verified in the present experiment. Instead, the vorticity in both models appears to be organized into several horizontal layers of like sign (in the lower part of the computational region at least), the vorticity center associated with the active cloud circulation being embedded in one of them. This is illustrated in figure 10, which, incidentally, has its sign convention opposite from Ogura's. The vorticity chart for the axisymmetric model shows a stronger principal maximum and more noise than that for the other model, but they are essentially similar.

Since the present run with the axisymmetric model was extended until the simulated cloud reached maturity and started to decay, it is of interest to look further into its life cycle. The computational region used by Ogura (and many of the other investigators) was limited to 3 km in depth, which precluded realistic development of the simulated cloud past the early growth stage.

The evolution of the simulated cloud in the present case is illustrated by figure 11, which shows the distribution of liquid water at various times from 10 to 50

370-724 O—70——4

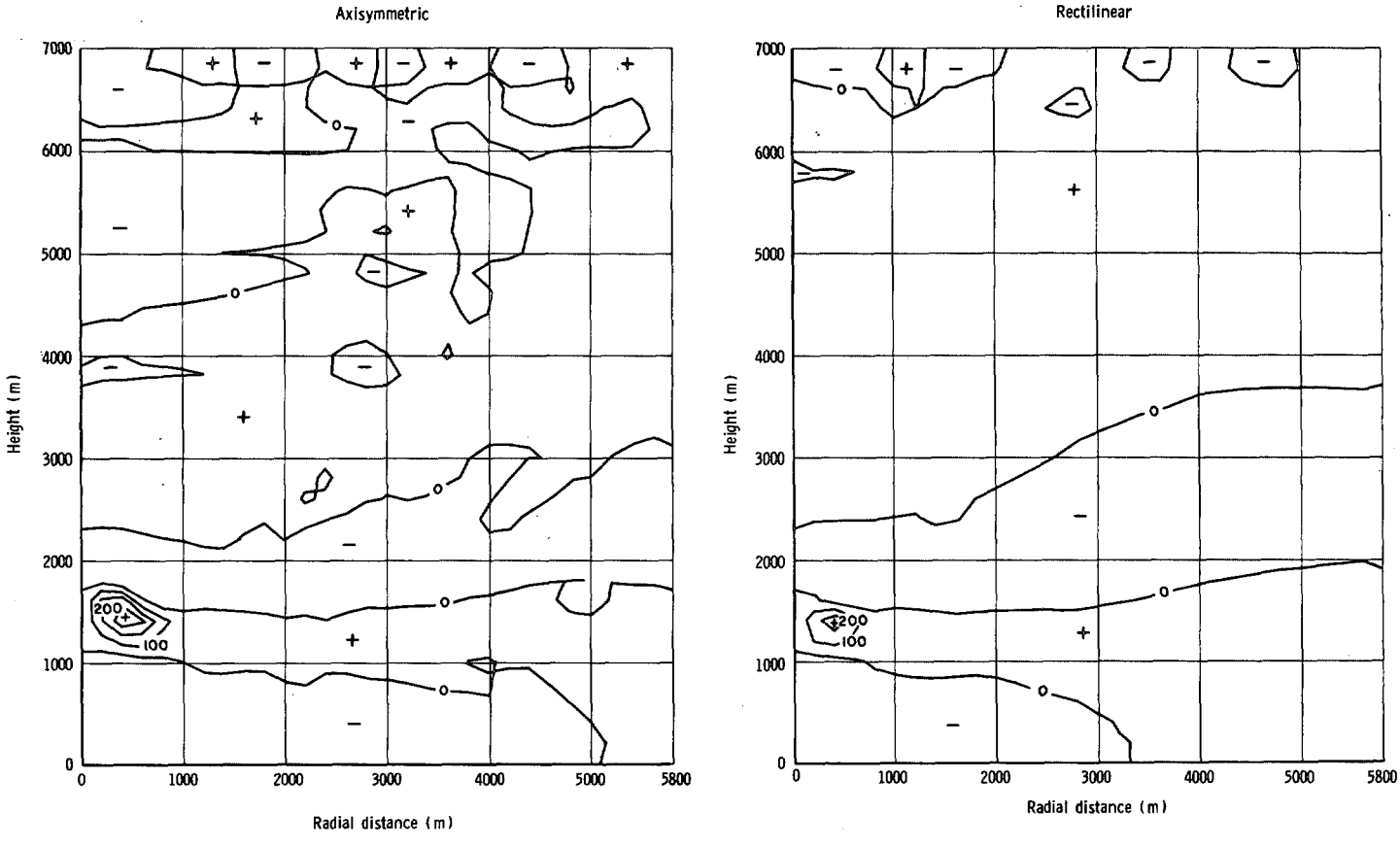


FIGURE 10.—Vorticity at 12 min, case of weak development.

min. Since the curve-drawing program automatically selects a contour interval appropriate to each diagram separately, the interval changes from time to time. The interval in grams per kilogram, designated by Δ, is shown at the top of each diagram. During the first 20 min the cloud has a globular shape, moderate radius, and rapidly increasing liquid content. During the next 10 min, when, according to figures 3 and 4, the maximum updraft is increasing and rising rapidly, the cloud also increases rapidly in depth and liquid content, but a mushroom shape becomes evident. By 38 min, the cloud top has reached its maximum height, but evaporation has caused a decrease in radius and liquid content. Over the next 6 min this process causes a dramatic collapse, as the upper half of the cloud vanishes. Thereupon growth resumes once more, suggesting the pulsation sometimes observed in natural clouds.

The circulations corresponding to these stages of cloud development are shown in figures 12A and 12B. During the growth stage (up to 30 min), the circulation is dominated by a circular vortex that remains closely associated with the cloud core. Toward the end of this period, however, other circulations of opposite sense appear and gain in importance; and by 38 min, downdrafts are found throughout the upper and outer parts of the cloud. This agrees with the rapid evaporation that occurs from 38 to 44 min. By 50 min, the second pulse is established, but its vortex is much weaker than that of the first pulse and is overshadowed by large circulations outside the im-

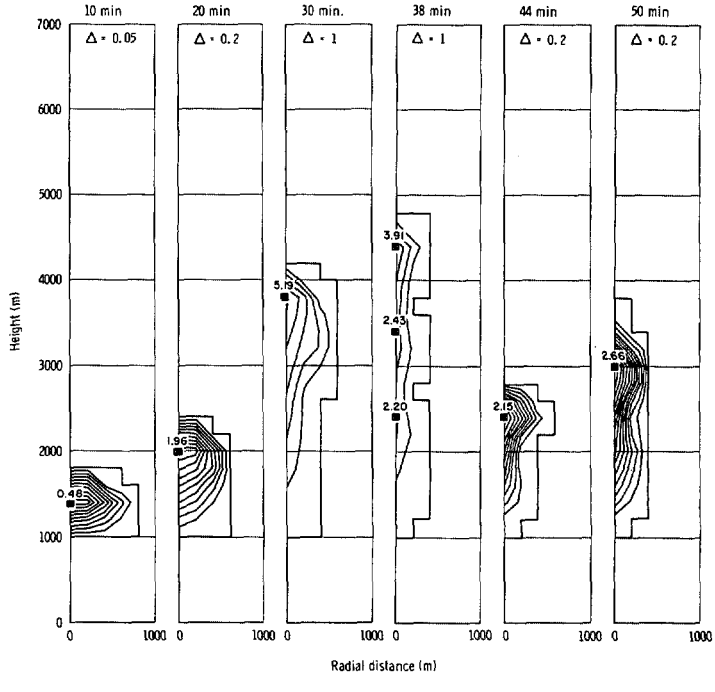


FIGURE 11.—Mixing ratio of liquid (gm $kg^{-1}$), axisymmetric case. Time and contour interval shown at top.

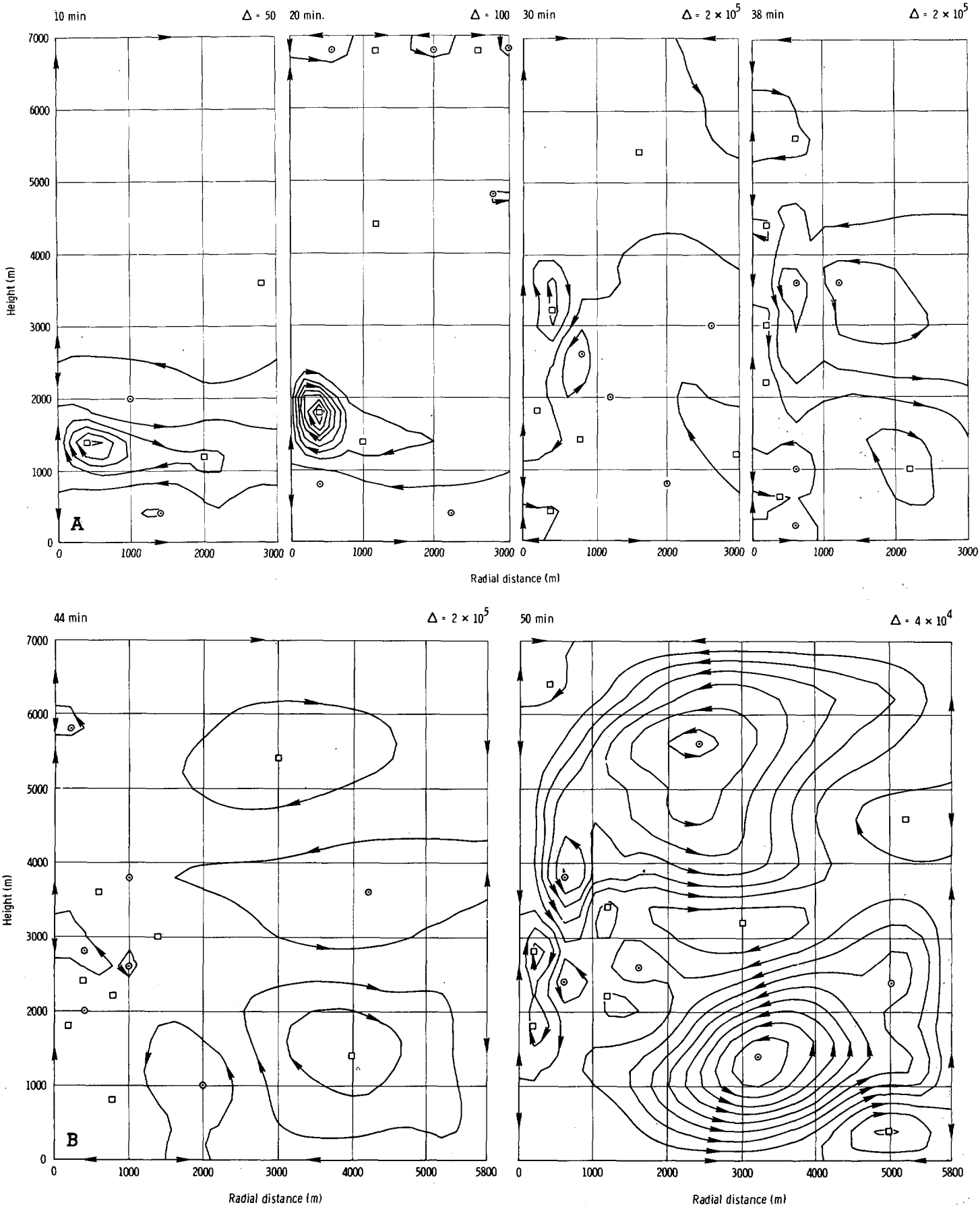


FIGURE 12.—Streamlines ($m^2$ $sec^{-1}$), axisymmetric case; time and contour interval shown at the top of (A) and (B); portions of the field more than 3 km from the axis have no interesting features and have been omitted in (A); the entire computational field is depicted in (B).

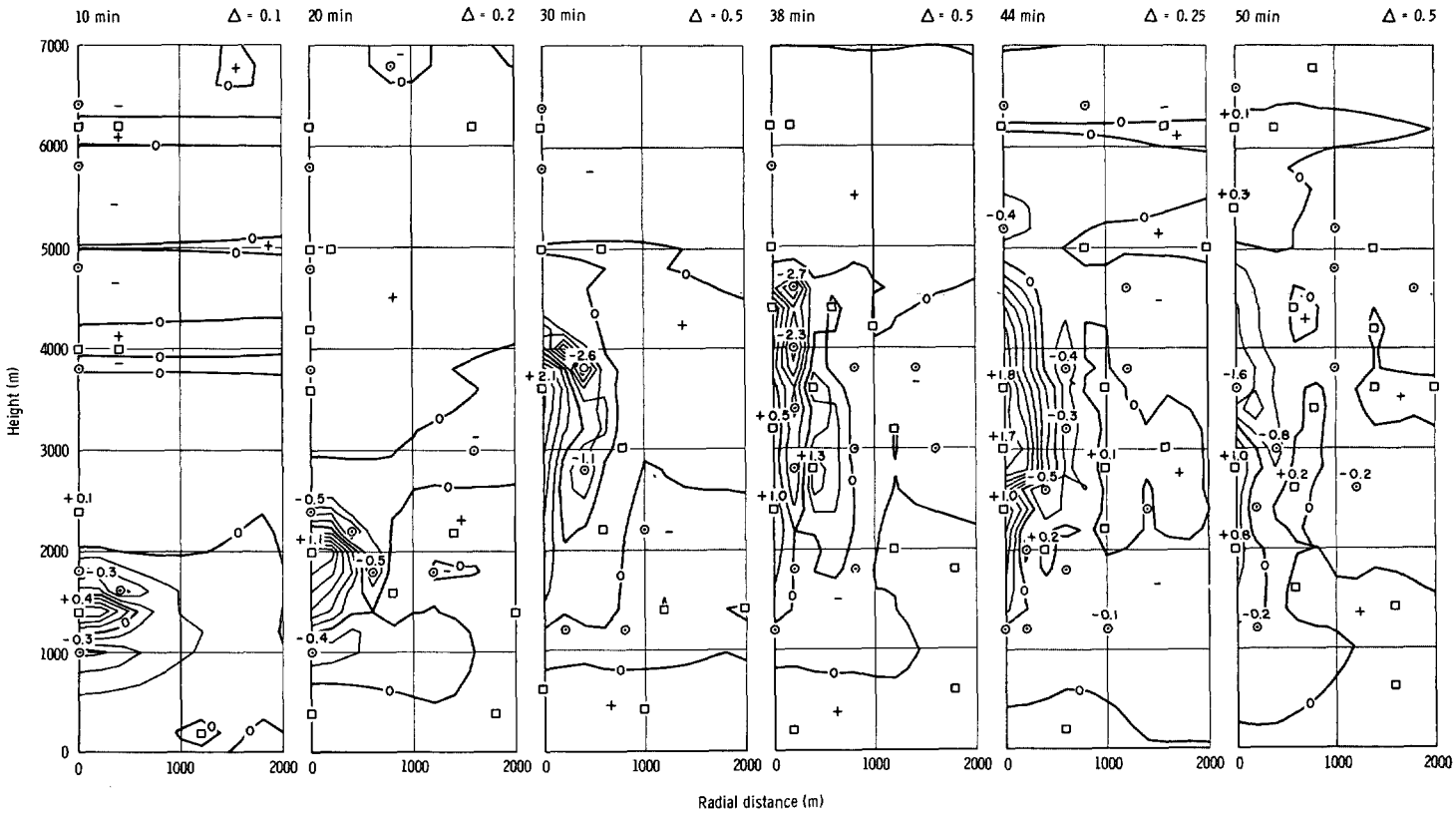


FIGURE 13.—Departure of temperature (°C) from the basic state, axisymmetric case; time and contour interval shown at the top; portions of the field more than 2 km from the axis have been omitted.

mediate cloud zone. The two main cells beyond 2-km radial distance reverse their directions between 44 and 50 min, but the maximum winds in them are only about 0.1 m $sec^{-1}$.

To complete the picture, the corresponding temperature departures are shown in figure 13. During the first 30 min an excess of temperature reaching as high as 2°C is associated with the body of the cloud, but above the cloud is a cold cap with a deficit of magnitude comparable to that of the excess within the cloud. The downdraft associated with the principal vortex results in evaporation along the outer edge of the cloud and consequently in reduction of the cloud radius and a downward extension of the cold cap, together with a movement of the center of maximum deficit away from the axis. By 38 min, there is a temperature deficit throughout all but the lowest part of the cloud as the upper part evaporates, but then dry-adiabatic heating in the downdraft along the axis produces a new excess. Thus, at 44 min there is an excess of 1°C in the cloud that is to start the second pulse and one of 1.8°C in the clear air above it. The latter, however, quickly becomes a deficit as the updraft is reestablished.

Taken together, the distributions of the several variables depict a cycle of growth, decay, and regrowth that is both qualitatively and quantitatively not unlike what is frequently observed in nature.

## 5. CONCLUSIONS

Despite certain fundamental differences between the two approaches, most notably in the computation of temperature and moisture content, Ogura's model and the present one give essentially similar results. In particular, Ogura's observations on the differences between models with axisymmetric and rectilinear symmetry are generally borne out by the present experiment, even though Ogura's comparative runs differed from each other in more than the basic geometry. Ogura, however, presented only fragmentary results of the comparison, whereas the present study involves a somewhat more systematic investigation into the effects of basic geometry on the model.

The principal conclusion reached by Ogura is that the downdraft is relatively stronger in the rectilinear model than in the axisymmetric. This is true also of the present study, for the ratio of maximum downdraft to maximum updraft is about .35 to .40 for the rectilinear model and near .15 for the other. These ratios are not constant with time, however, and their physical significance seems to change about the eighth minute. At later times, however, the comparisons are consistent.

What is even more striking than the difference in ratio of downdraft to updraft is the difference in speed

and strength of development. In the present experiment the axisymmetric model showed much stronger updrafts than the rectilinear, and consequently its model cloud was both bigger and wetter. In this instance, at least, the difference favored the axisymmetric model, for clouds of the size and strength predicted by it were characteristic of the real situation as observed in nature.

To an extent that has not yet fully been determined, the rate of development of both axisymmetric and rectilinear models is influenced by the size, strength, and nature of the initial impulse. This will be discussed at greater length in another report, but briefly it has been noted that a deep humidity impulse will result in a very strong and rapid development. In many cases the updraft increases so rapidly that it soon exceeds reasonable values, requiring termination of computation. This is true of both geometries, but is particularly troublesome for the axisymmetric model. The arbitrary addition of water vapor to a closed system, which characterizes the humidity impulse, is equivalent to the addition of energy. If the impulse is large, the added energy may represent a significant fraction of the energy already latent in the system, so that the impulse, rather than the characteristics of the undisturbed atmosphere, dominates the later development. In the present experiment the impulse was small, and realistic development resulted.

The nature of the impulse is important. The conventional impulse is one of temperature. The size of a temperature impulse is less critical than that of a humidity impulse, but it has other disadvantages, among these being a greater tendency toward extreme mushroom shape and development of a low-level reverse cell. Ogura, using a temperature impulse, noted a distinct difference in the vorticity patterns with the two geometries and development of a reverse cell below the cloud in the rectilinear model but not in the axisymmetric. In the present experiment there is not much difference in the vorticity and streamline patterns between the models, though magnitudes and spacings differ strongly. There is some evidence that when run with a temperature impulse the present model gives results more like those of Ogura in this respect. On the whole, though, it appears that the humidity impulse leads to more realistic results, so it has been retained.

From the standpoint of realism the present model, particularly the axisymmetric version, appears to be very satisfactory. Reference to table 1 shows that its properties are well within the range observed in nature. Moreover, it has been found capable of carrying a simulation through the mature and decaying stages of cumulus development to the appearance of a second pulse. Some improvements, of course, are in order. Among these would be the inclusion of a precipitation mechanism to reduce the sometimes large liquid water content in the uppermost part of the cloud. It should be noted, however, that typically the maximum updraft is stronger than the relative fall rate of large rain drops, so that even with a precipitation mechanism there should be a concentration of liquid water at the level of maximum updraft. But this in turn would contribute to a reduction in buoyancy and in updraft strength. In any case it is apparent that the two geometries give strongly different results in some respects, and that in most respects the axisymmetric model more accurately simulates a real tropical cumulus.

## 5. APPENDIX

Let $\varphi$ represent any of the primary variables (for example, pressure). Then by definition $\varphi=\bar{\varphi}+\varphi_B+\varphi'$ where $\bar{\varphi}$ is the (constant) mean value of $\varphi$ over the entire computational region at initial time in the absence of motion. $\varphi_B=\varphi_B(z)$ is the departure of $\varphi$ from $\bar{\varphi}$ at a given height $z$ at initial time in the absence of motion, and $\varphi'=\varphi'(x, z, t)$ is the departure of $\varphi$ from $\bar{\varphi}+\varphi_B$ at any location $(x, z)$ and any time $t$.

The symbols used in this report have the following meanings:

*Scalars*

$B$=buoyancy parameter
$L$=latent heat of condensation
$R$=gas constant for dry air
$T$=temperature
$T^*$=virtual temperature
$c_p$=specific heat of dry air at constant pressure
$c_{pv}$=specific heat of water vapor at constant pressure
$c_w$=specific heat of liquid water
$e_s$=saturation vapor pressure
$g$=acceleration due to gravity
$p$=pressure
$r_l$=mixing ratio of liquid water to dry air
$r_s$=saturation mixing ratio
$r_v$=mixing ratio of water vapor to dry air
$t$=time
$u$=horizontal component of wind
$w$=vertical component of wind
$x$=radial coordinate
$z$=vertical coordinate
$\alpha$=specific volume
$\epsilon$=ratio of molecular weights of water vapor and dry air
$\eta$=horizontal component of vorticity
$\nu_M$=coefficient of eddy transport of momentum
$\nu_r$=coefficient of eddy diffusion of water substance
$\nu_T$=coefficient of eddy diffusion of temperature
$\psi$=stream function

*Vectors*

$\mathbf{v}$=wind velocity
$\mathbf{k}$=vertical unit vector
$\boldsymbol{\omega}$=vorticity

## REFERENCES

Amirov, A. D., "O razvitii termikov i kuchevyh oblakov v stratifitsirovannoĭ atmosfere," (Development of Thermals and Cumulus Clouds in a Stratified Atmosphere), *Fizika Atmosfery i Okeana*, Vol. 2, No. 5, Izvestiia Akademiia Nauk SSSR, May **1966***a*, pp. 449–463.

Amirov, A. D., "O roli turbulentnosti v konvektivnom dvizhenii," (Role of Turbulence in Convective Motion), *Fizika Atmosfery i Okeana*, Vol. 2, No. 7, Izvestiia Akademiia Nauk SSSR, July **1966***b*, pp. 705–713.

Árnason, G., Greenfield, R. S., and Newburg, E. A., "A Numerical Experiment in Dry and Moist Convection Including the Rain Stage," *Journal of the Atmospheric Sciences*, Vol. 25, No. 3, May **1968**, pp. 404–415.

Asai, T., "Numerical Experiment of Cumulus Convection Under the Pseudo-Adiabatic Process," *Papers in Meteorology and Geophysics*, Vol. 15, No. 1, Tokyo, Apr. **1964***a*, pp. 1–30.

Asai, T., "Cumulus Convection in the Atmosphere With Vertical Wind Shear: Numerical Experiment," *Journal of the Meteorological Society of Japan*, Ser. 2, Vol. 42, No. 4, Aug. **1964***b*, pp. 245–259.

Berkovsky, L., "The Inclusion of Latent Heat of Condensation in a Numerical Forecasting Model," *Cumulus Dynamics*, Pergamon Press, New York, **1960**, pp. 85–102

Bjerknes, J., "Saturated-Adiabatic Ascent of Air Through a Dry Adiabatically Descending Environment," *Quarterly Journal of the Royal Meteorological Society*, Vol. 64, **1938**, pp. 325–330.

Chou, H.-P., "Development of Cumulus Clouds," (K voprosy o razvitii kuchevykh oblakov, Apr. 1962), J. S. Sweet, Translator, *Bulletin (Izvestiia) of the Academy of Sciences, USSR, Geophysics Series, No. 4*, American Geophysical Union, Washington, D.C., July **1962**, pp. 358–363.

Chou, H.-P., Li, H.-S., Chang, Y.-K., and Kung, T.-C., "Numerical Experiment of Cumulus Development," (translation from Acta Meteorologica Sinica, Vol. 34, Nov. 1964, pp. 475–484), *Translations on Communist China: Science and Technology*, No. 233, U.S. Department of Commerce, Joint Publications Research Service 32,737, Washington, D.C., Nov. 5, **1965**, pp. 33–51.

Inman, R. L., "The Evolution of Convective Motions in a Rotating Fluid: A Numerical Calculation," Ph. D. dissertation, Texas A&M University, College Station, **1966**, 90 pp.

Kessler, E., III, "On the Continuity of Water Substance, Model Circulations With Microphysical Processes," *ESSA Technical Memorandum* IERTM–NSSL 33, U.S. Department of Commerce, National Severe Storms Laboratory, Norman, Okla., Apr. **1967**, 125 pp. (see pp. 1–85).

Krishnamurti, T. N., "A Calculation of Percentage Area Covered by Convective Clouds From Moisture Convergence," *Journal of Applied Meteorology*, Vol. 7, No. 2, Apr. **1968**, pp. 184–195.

Lebedev, S. L., "Trekhmernaia nestatsionarnaia model' atmosfernoĭ konvektivnoĭ iacheĭki s oblakom," (Three-Dimensional Nonstationary Model of an Atmospheric Convection Cell With Clouds), *Fizika Atmosfery i Okeana*, Vol. 2, No. 1, Izvestiia Akademiia Nauk SSSR, Jan. **1966**, pp. 14–27.

Li, S.-S., Chao, J.-P., and Hwu, Y.-C., "Dynamical Analysis of the Development of the Cumulo Nimbus Incus," *Acta Meteorologica Sinica*, Vol. 34, No. 2, May **1964**, pp. 225–232.

Lilly, D. K., "On the Numerical Simulation of Buoyant Convection," *Tellus*, Vol. 14, No. 2, May **1962**, pp. 148–172.

Malkus, J. S., and Witt, G., "The Evolution of a Convective Element: A Numerical Calculation," *The Atmosphere and the Sea in Motion*, Rockefeller Institute Press, New York, **1959**, pp. 425–439.

Molenkamp, C. R., "Accuracy of Finite-Difference Methods Applied to the Advection Equation," *Journal of Applied Meteorology*, Vol. 7, No. 2, Apr. **1968**, pp. 160–167.

Murray, F. W., and Anderson, C. E., "Numerical Simulation of the Evolution of Cumulus Towers," *Report* SM–49230, Douglas Aircraft Company, Inc., Santa Monica, Calif., Oct. **1965**, 97 pp.

Murray, F. W., and Hollinden, A. B., "The Evolution of Cumulus Clouds: A Numerical Simulation and Its Comparison Against Observations," *Final Report* SM–49372, Contract No. Nonr–4715(00)(X), Douglas Aircraft Company, Inc., Santa Monica, Calif., Mar. **1966**, 147 pp.

Nickerson, E. C., "A Numerical Experiment in Buoyant Convection Involving the Use of a Heat Source," *Journal of the Atmospheric Sciences*, Vol. 22, No. 4, July **1965**, pp. 412–418.

Ogura, Y., "Convection of Isolated Masses of a Buoyant Fluid: A Numerical Calculation," *Journal of the Atmospheric Sciences*, Vol. 19, No. 6, Nov. **1962**, pp. 492–502.

Ogura, Y., "The Evolution of a Moist Convective Element in a Shallow, Conditionally Unstable Atmosphere: A Numerical Calculation," *Journal of the Atmospheric Sciences*, Vol. 20, No. 5, Sept. **1963**, pp. 407–424.

Ogura, Y., and Charney, J., "A Numerical Model of Thermal Convection in the Atmosphere," *Proceedings of the International Symposium on Numerical Weather Prediction, Tokyo, Japan, Nov. 7–13, 1960*, Meteorological Society of Japan, Tokyo, Mar. **1962**, pp. 431–451.

Orville, H. D., "A Numerical Study of the Initiation of Cumulus Clouds Over Mountainous Terrain," *Journal of the Atmospheric Sciences*, Vol. 22, No. 6, Nov. **1965**, pp. 684–699.

Orville, H. D., "Ambient Wind Effects on the Initiation and Development of Cumulus Clouds Over Mountains," *Journal of the Atmospheric Sciences*, Vol. 25, No. 3, May **1968**, pp. 385–403.

Petterssen, S., "Contribution to the Theory of Convection," *Geofysiske Publikasjoner*, Vol. 12, No. 9, **1939**, 23 pp.

Simpson, J., Atmospheric Physics and Chemistry Laboratory, ESSA, Miami, Fla., **1968**, (personal communication).

Simpson, J., Simpson, R. H., Andrews, D. A., and Eaton, M. A., "Experimental Cumulus Dynamics," *Reviews of Geophysics*, Vol. 3, No. 3, Aug. **1965**, pp. 387–431.

Takeda, T., "The Downdraft in Convective Shower-Cloud Under the Vertical Wind Shear and Its Significance for the Maintenance of Convective System," *Journal of the Meteorological Society of Japan*, Ser. 2, Vol. 43, No. 6, Dec. **1965**, pp. 302–309.

Vul'fson, N. I., "Effect of Air Humidity on Development of Convection in a Cloudless Atmosphere," (Vliyaniye vlazhnosti vozdukha na razvitiye konvektivnykh divzheniy v bezoblachnoy atmosfere, July–Aug. 1963), *Doklady Akademiia Nauk SSSR, Earth Science Sections, Vol. 151, July–Aug. 1963*, (Translation), American Geological Institute, Washington, D.C., Mar. **1964**, pp. 10–12.

*[Received April 15, 1969; revised August 18, 1969]*